Method for Calculating Aerodynamic Heating on Sounding Rocket Tangent Ogive Noses

L. D. WING*
NASA Goddard Space Flight Center, Greenbelt, Md.

A method is presented for calculating the aerodynamic heating and shear stresses at the wall for tangent ogive noses that are slender enough to maintain an attached nose shock through that portion of flight during which heat transfer from the boundary layer to the wall is significant. The lower entropy of the attached nose shock combined with the inclusion of the streamwise pressure gradient yields a reasonable estimate of the actual flow conditions. Both laminar and turbulent boundary layers are examined. The angle of attack is zero as is the usual case for sounding rocket ascent.

Nomenclature

C_f = friction coefficient (local) (−)
C_p = specific heat of air, Btu/lbm °K
$(dV/dx)_{(0)}$ = Newtonian velocity gradient at the stagnation point on a circular nose, sec^{-1} Eq. (19)
$f''_{(w)}$ = velocity gradient parameter,[6] Eqs. (27) and (28)
g = acceleration of gravity, 32.174 ft/sec^2
h, h^* = enthalpy and reference enthalpy, respectively, Btu/lbm
$H^*_{(0)}, H^*_{(x)}$ = defined by Eqs. (18) and (17), respectively
k = coefficient of thermal conductivity, Btu/ft sec °K
N = a constant; set = 0 for one-dimensional flow; set = 1 for axisymmetric flow, = 1 throughout this program
Nu = Nusselt number (−)
$P(I)$ = pressure at stations 1–15, atmospheres, except where otherwise noted
Pr = Prandtl number (−)
$PXPO(I)$ = the local to stagnation point pressure ratio at each of the 15 station locations (−)
$\dot{q}$ = heat transfer rate, Btu/ft^2 sec
R = tangent ogive radius of curvature (Figs. 1 and 2) (ft)
Re or $Re_{(x)}$ = local Reynolds number, Eq. (25) (−)
$Re_{(\theta)}$ = local momentum thickness Reynolds number, Eq. (26) (−)
R_N = spherical nose radius (for calculations of blunt body stagnation point heat transfer rate), ft
$r(i)$ or $r(x)$ = the flow deflection distance defined by Eq. (11) and shown in Figs. 1 and 2, ft
V = velocity, fps
x' = tangent ogive longitudinal dimension (shown in Figs. 1 and 2), ft
$S(i)$ = surface coordinate distance along streamline from nose tip to each station, ft
y' = tangent ogive base radius, shown in Figs. 1 and 2, ft
δcr = the flow deflection angle (conical flow) at which the nose shock becomes detached for a given freestream Mach number, deg or rad
θ = the local surface deflection angle; also, the central angle turned by the tangent ogive radius, R, to define the complete ogive (see Figs. 1 and 2), deg or rad
θ_c = cone half-angle, deg or rad
μ = viscosity coefficient, lbf sec/ft^2
ρ = density of air, lbm sec^2/ft^4 = slugs/ft^3
τ = boundary layer shear stress at the wall, lbf/ft^2
$\phi(i)$ = angle defined by Eq. (10) and shown in Fig. 2, deg or rad

Subscripts

e = local external-to-boundary-layer value
lam = considers a laminar boundary layer
rec = evaluated at recovery conditions
ref = evaluated at reference conditions (see superscript)
turb = considers a turbulent boundary layer
X = at a position X feet from nose tip along a surface streamline (same as e or S)
w = evaluated at local pressure and wall temperature
o = at stagnation point for a spherical nose of radius, R_N
∞ = freestream (ahead of nose shock) value

Superscript

$*$ = property evaluated at local pressure and reference enthalpy

Presented as Paper 73-281 at the AIAA 3rd Sounding Rocket Technical Conference, Albuquerque, N.Mex., March 7–9, 1973; submitted April 2, 1973; revision received December 27, 1973.

Index categories: LV/M Aerodynamic Heating; Boundary Layers and Convective Heat Transfer—Laminar and Turbulent.

* Aerospace Engineer, Sounding Rocket Division. Member AIAA.

Introduction

THE generally favorable aerodynamic characteristics of the tangent ogive in supersonic and hypersonic flow result in the common use of this configuration for sounding rocket noses. Accordingly, an analytical method for calculating the aerodynamic heating on such configurations has been devised, combining basic analytical methods which are well known with some which are less common and with certain basic assumptions. These methods, while approximate in nature, yield results which have proved to be adequate for the design of both the structure of the rocket nose and the protection of payload items within. The entire analysis described here has been programed in FORTRAN IV for an IBM 360/91 system.[1]

The slenderness of the ogives of interest results in an attached nose shock wave through periods of supersonic and hypersonic flight during which significant aerodynamic heating is experienced. The low entropy jump across the oblique shock wave as opposed to the entropy jump across the normal shock wave associated with "blunt bodies" results in an increase of heat transfer to the ogive for a constant flight condition. This is similar to the case of the cone heating as compared to that on a blunt, axisymmetric body. However, unlike the cone case, the ogive body has a definite (first-order) pressure gradient along the surface streamlines. A blunt body analysis is treated in Ref. 2 and a conical body analysis in Ref. 3. The present analysis considers the in-between (tangent ogive) case in which the nose shock is oblique but there is a body pressure gradient.

Theory

The theory is derived from a combination of the analytical methods of Refs. 2 and 3 with several new approximations and assumptions. The pertinent geometry, along with the most important items of nomenclature, are shown in Figs. 1 and 2. The tangent ogive and flow geometry are completely defined by the parameters x' and y' (identified in Fig. 1) in conjunction with the geometric Eqs. (7–12). The applicable freestream conditions are derived either from the vehicle altitude and any

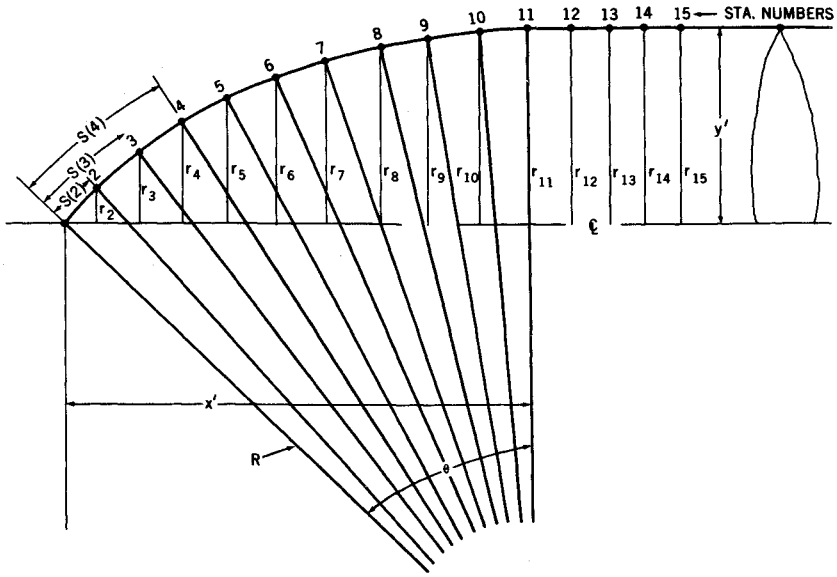

Fig. 1 Geometry of tangent ogive nose.

appropriate ARDC atmosphere or by electing to define the prenose shock air properties by specifying two thermodynamic variables, the pressure and the temperature, then obtaining all the other properties from the real gas (equilibrium) Mollier approximations of Hansen.[4]

For simplicity, a fixed number of body locations are specified for each problem. Either of two procedures can be adopted for defining the local flow conditions at these specified 15 body points. In the first case, the local pressures at the calculation points are defined by Newtonian approximations or from experiment (if available). The entropy behind the attached nose shock (assumed to be conical) is then calculated using the actual local surface angle. The local external-to-boundary-layer properties are defined by isentropically expanding to the given local pressures. This assumes that the entropy is constant at the postnose shock value over the entire body and results in an overprediction of the available energy, hence, heat transfer rate to the wall. The second method obtains the postnose shock entropy and pressure (as in the first method) and taking these data as initial values, uses a Prandtl-Meyer expansion through $\Delta\theta°$ to get the pressure at point 2 (Fig. 1). This pressure and the point 1 entropy are then used with air properties[4] to define all external-to-boundary-layer properties at point 2. The local surface angle at point 2 is then considered to be the cone half-angle and a new cone (external-to-boundary layer) entropy at point 2 is calculated and used in the same manner as just described to expand by an appropriate Prandtl-Meyer routine through $\Delta\theta°$ to obtain the point 3 pressure at the point 2 entropy. In this way, the properties at each point on the ogive are approximated by using the entropy of the immediate upstream point.

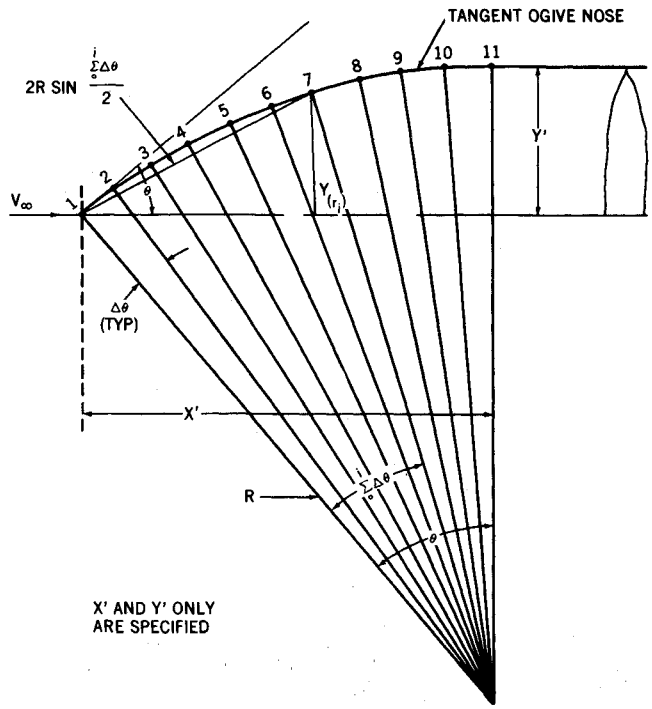

Fig. 2 Definitions of math symbols.

This method represents an attempt to approximate the entropy gradient across the shock layer. Note that the entropies so derived are conservatively lower the farther aft one goes on the ogive. Moreover, the greatest conservatism in the predictions of the local heat transfer rate occurs at point 11. For all points downstream of 11, the entropy is left at the point 11 calculated value and the pressures are assumed to be the arithmetic average of the freestream (ahead of the nose shock) and the point just upstream of the point being studied. Mathematically

$$SR(11) = SR(12) = SR(13) = SR(14) = SR(15) \quad (1)$$

and

$$P(11) = (P_\infty + P(10))/2 \quad (2)$$
$$P(12) = (P_\infty + P(11))/2 \quad (3)$$
$$P(13) = (P_\infty + P(12))/2 \quad (4)$$
$$P(14) = (P_\infty + P(13))/2 \quad (5)$$
$$P(15) = P_\infty \quad (6)$$

Of course, the Prandtl-Meyer expansion is used only up to and including point 11. From point 11 to points 12, 13, 14, and 15, the entropy is constant and isentropic expansion to the local pressures indicated in Eqs. (2–6) defines the local flow properties. The calculated pressure is not allowed to go below 80% of the freestream pressure, as would sometimes result from the Prandtl-Meyer expansion technique described.

It should be emphasized that while the entropy values for the second method are low (yielding conservatively high heat transfer rates), the pressures that result from the Prandtl-Meyer expansion technique are also normally on the low side. This tends to decrease the predicted heat transfer rates. The two effects tend to offset each other.

Geometric Calculations

The programing of the analysis is greatly simplified by the fact that a fixed number of stations on a fixed geometry (the tangent

ogive followed by a cylinder) are treated. In specifying the magnitude of x' and y' all necessary geometric input has been supplied and one is able to generate the geometric details required by means of the following equations (the nomenclature of which is defined in Fig. 2): given only x' and y'

$$R = (x'^2 + y'^2)/2y' \tag{7}$$

$$\theta = \tan^{-1} x'/(R - y') = \tan^{-1} 2x'y'/(x'^2 - y'^2) \tag{8}$$

$\Delta\theta$ is defined as

$$\Delta\theta = 0.1(\theta) \tag{9}$$

To calculate the "flow deflection" distance, $r(i)$, define

$$\phi(i) = PHI(i) = \theta - \left(\sum_0^i \Delta\theta \Big/ 2\right) \tag{10}$$

and then (from the right triangle of Fig. 2)

$$r(i) = 2R \sin\left(\sum_0^i \Delta\theta \Big/ 2\right) \sin\phi(i) \tag{11}$$

The surface coordinate distance (boundary-layer build-up distance) is

$$S(i) = R\sum_1^i \Delta\theta_i \tag{12}$$

Assumptions

The following basic assumptions are applicable to the analytical methods:

1) The shock layer entropy gradient effect on the external-to-boundary-layer flow properties along the ogive is approximated by assuming the local external flow to have originated just downstream of a shock wave generated by a cone of the same half-angle as the local surface angle. This tends to predict increasingly lower (than the true local value) entropies as one considers points farther downstream on the ogive. The predicted heat transfer, therefore, is expected to become increasingly conservative as the farther downstream stations are treated.

2) In the alternate method in which pressures are input and the entropy is constant at the postnose shock (point 1) value, the calculated entropy is expected to be higher than the actual values for downstream points, again the error growing with distance downstream. Accordingly, lower heat transfer rates downstream should result from the entropy effect of the pressure-input option. Note that one cannot conclude from this that the heat rate distributions from this method are actually conservative because their magnitudes in this option are also highly dependent upon the magnitudes of the pressures that are input. The above remarks refer to the entropy effect alone (as though the pressures by either method were equal).

Heat Transfer Rate and Shear Stress on Body

The boundary-layer heat transfer rate and shear stresses at the wall are calculated by means of a) the Eckert and Tewfik adaptation of Lee's momentum integral equation[5] and the use of Reynolds analogy for the laminar case, and b) the Flat Plate Reference Enthalpy Method[6] (also applying Reynolds analogy) for the turbulent boundary-layer case. These equations are

1) Laminar heat rate (ratioed to the spherical nose stagnation point heat rate)[5]

$$\frac{\dot{q}(x)}{\dot{q}(0)} = \left[\frac{k^*_{(x)}}{k^*_{(0)}}\right]\left[\frac{H^*_{(x)}}{H^*_{(0)}}\right]\left[\frac{h_{\text{rec}} - h_{(w)}}{h_{(0)} - h_{(w)}}\right]\left[\frac{Cp_{w(0)}}{Cp_{w(x)}}\right] \tag{13}$$

where the starred quantities are evaluated at local pressure and reference enthalpy, h^*.

$$h^* = h_{\text{ref}} = \frac{h_{(e)} + h_{(w)}}{2} + 0.22(Pr_{(e)})^{1/2}(h_{(0)} - h_{(w)}) \tag{14}$$

$$h_{\text{rec}} = h_{(e)}[1 - (Pr^*)^{1/2}] + h_{(0)}(Pr^*)^{1/2} \text{ (laminar B.L.)} \tag{15}$$

or

$$h_{\text{rec}} = h_{(e)}[1 - (Pr^*)^{1/3}] + h_{(0)}(Pr^*)^{1/3} \text{ (turbulent B.L.)} \tag{16}$$

In Eq. (13), $H^*(x)$ is given by

$$H^*_{(x)} = \left[\frac{\rho^*_{(x)}}{\rho^*_{(0)}}\right]\left[\frac{V_{(x)}}{V_{(\infty)}}\right](r(x))^N \left\{\int_0^x \left[\frac{\rho^*_{(x)}\mu^*_{(x)}}{\rho^*_{(0)}\mu^*_{(0)}}\right]\left[\frac{V_{(x)}}{V_{(\infty)}}\right](r(x))^{2N}\, dx\right\}^{1/2} \tag{17}$$

$N = 0$ for two-dimensional and $N = 1$ for axisymmetric flow (hence $N = 1$ for the case considered) and

$$H^*_{(0)} = \left[\frac{(2\rho^*_{(x)}/\rho^*_{(0)})(dV/dx)_0}{V_\infty(\mu^*_{(x)}/\mu^*_{(0)})}\right]^{1/2}(1+N)^{1/2} \tag{18}$$

is the stagnation point value.

Note that $(dV/dx)_{(0)}$ is given the Newtonian (circular nose) value

$$\left(\frac{dV}{dx}\right)_0 = \frac{(2)^{1/2}}{R_N}\left[\frac{p_{(0)} - p_{(\infty)}}{\rho_{(0)}}\right]^{1/2} \tag{19}$$

The turbulent heating equation[6] is

$$\dot{q}_{\text{turb}} = \{0.03(g)^{1/3}(1+N)^{0.2}(k^*_{(x)})^{2/3}(\rho^*_{(x)}V_{(x)})^{0.8}[(1-(p_r^*)^{1/3}h_{(x)} + (p_r^*)^{1/3}h_{(0)} - h_{(w)}]\}/(\mu^*_{(x)})^{7/15}(C^*_{p(0)})^{2/3}x^{0.2} \tag{20}$$

Using Reynolds analogy, the laminar and turbulent shear stress and friction coefficients are calculated from

$$C_{f\text{lam}} = \frac{2\dot{q}_{\text{lam}}(Pr^*_{(x)})^{2/3}}{\rho_{(x)}V_{(x)}(h_{\text{rec}} - h_{(w)})g} \tag{21}$$

$$C_{f\text{turb}} = \frac{2\dot{q}_{\text{turb}}(Pr^*_{(x)})^{2/3}}{\rho_{(x)}V_{(x)}(h_{\text{rec}} - h_{(w)})g} \tag{22}$$

$$\tau_{\text{lam}} = 0.5C_{f\text{lam}}\rho_{(x)}V^2_{(x)} \tag{23}$$

$$\tau_{\text{turb}} = 0.5C_{f\text{turb}}\rho_{(x)}V^2_{(x)} \tag{24}$$

The local Reynolds number is calculated from

$$Re_{(x)} = (\rho_{(x)}V_{(x)}X)/\mu_{(x)} \tag{25}$$

and the momentum thickness Reynolds number[2] is

$$Re_{(\theta)} = 0.87f''_{(w)}\rho_{(w)}\mu_{(w)}/C_{f(w)}\rho_{(x)}\mu_{(x)} \tag{26}$$

in which the Cohen and Reshotko's[7] velocity gradient parameter, $f''_{(w)}$, is curve-fitted by the following two equations (valid for favorable pressure gradients):

a) $C_f R_e/N_u > 2$

$$f''_{(w)} = 0.0508[C_f R_e/N_u]^2 + 0.1332[C_f R_e/N_u] \tag{27}$$

b) $0 \leqq C_f R_e/N_u \leqq 2$

$$f''_{(w)} = 0.011627[C_f R_e/N_u]^2 + 0.25644[C_f R_e/N_u] - 0.089787 \tag{28}$$

Shock and Expansion Routines

The real gas oblique shock routine for hypersonic flow and the method of accounting for the pressure and entropy gradients across the shock layer for conical flow are given in Appendix B, Ref. 3. This hypersonic analysis (real gas in equilibrium) becomes invalid in the medium to low supersonic range so an alternate supersonic conical shock calculation method, perfect gas (see Appendix C, Ref. 3) is available upon failure of the hypersonic analysis.

Similarly, a real gas (applicable for hypersonic Mach number ranges) Prandtl-Meyer expansion routine (Fig. 4, Ref. 2) is valid only down to local Mach numbers somewhere between 2 and 3. As with the cone shock calculations, the real gas Prandtl-Meyer analysis is backed up by a perfect gas routine (Appendix D, Ref. 3) which is used when failure of the real gas method occurs. Note that in either the shock or expansion analysis for low supersonic flow, the perfect gas assumption is quite valid.

Hemispherical Nose Stagnation Heating

There are two reasons for including the calculation of the hemispherical nose calculation in this analysis. First, the postnormal shock flow properties are required for the laminar boundary-layer heat rate calculation of Eq. (13) and, in the same equation, the stagnation heat rate is specifically required to re-dimensionalize the heat ratio to get the absolute value of the

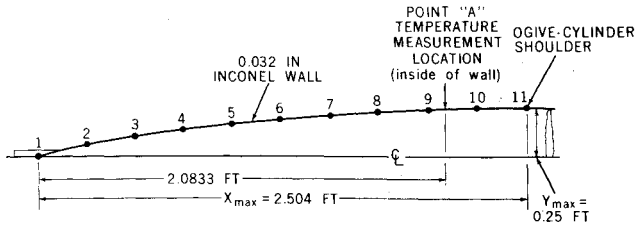

Fig. 3a Sketch of the vehicle nose for NASA TND889.

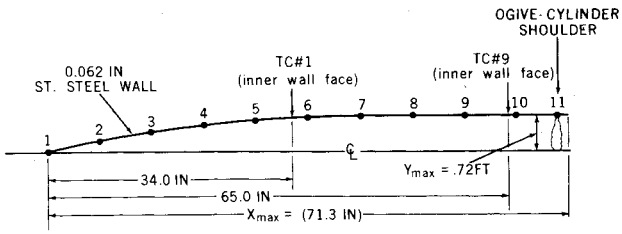

Fig. 3b Sketch of Black Brant VC nose showing locations of thermocouples.

local laminar heat rate. The second reason lies in the fact that the stagnation point heat transfer is often desired as a general heat transfer parameter for evaluating the effects of trajectory parameters, vehicle weight, etc., upon the vehicle thermal environment.

Note that the nose radius selected for the calculation enters into the solution of Eq. (13) only via the $H^*_{(0)}$ term, Eq. (18), in the form of the stagnation point velocity gradient, Eq. (19). The same nose radius is also used in the stagnation point heating rate, Eq. (29), so it is clear that all data relative to body points 1–15 are totally independent of the value of R_N. For this reason it is suggested that a value of $R_N = 1$ ft be assumed because this is commonly used as a heat indicator.

The stagnation point heat rate can be calculated by the equation of Fay and Riddell[8] with the Lewis number assumed equal to unity

$$\dot{q}_{\text{stag·point}} = 0.76g(Pr)^{-0.6}(\rho_{(w)}\mu_{(w)})^{0.1}(\rho_{(x)}\mu_{(x)})^{0.4} \times (h_{(0)} - h_{(w)})[(dV/dx)_0{}^{1/2}] \quad (29)$$

Detachment of Nose Shock Wave

The method of estimating the point 1 conditions by assuming the conical nose shock wave that would result from a cone of half-angle equal to the angle shown as θ in Fig. 2 does introduce a possible problem. If θ at any given freestream Mach number is greater than some critical flow deflection angle, δ_{cr}, the nose shock will detach and the analytical methods will become invalid. In order to protect against this possibility (which can arise from too blunt an ogive) the critical conical flow deflection angle as a function of freestream Mach number is taken from chart 5 of Ref. 9. Thus, for each problem, the nose apex flow deflection angle and the freestream Mach number are known. The analyst uses the freestream Mach number in the appropriate region of Fig. 5 of Ref. 9 to obtain the maximum allowable flow deflection angle, δ_{cr}. This angle is then compared with the actual deflection angle, θ, at the nose and if $\delta_{cr} < \theta$, it is clear that the shock is detached and the present analysis is inapplicable.

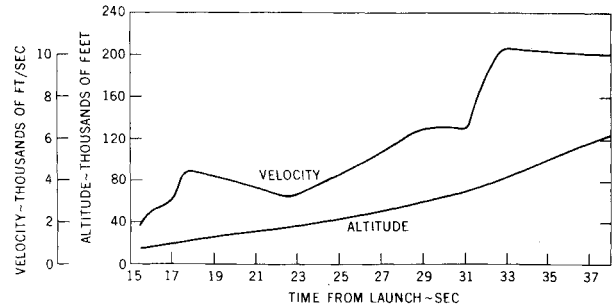

Fig. 4 Velocity and altitude histories for the flight of the vehicle of Fig. 3a through the significant aeroheating portion of flight.

Comparison of Theory with Flight Data

In order to test the theory presented here with flight data, two cases are considered: a four-stage vehicle[10] and Black Brant VC, Flight 21.006 GT.

1) Comparison with Flight Data from NASA TND 889

The vehicle nose of Fig. 3a was flown on a four-stage vehicle[10] with a temperature history measured on the inside of the 0.032 in. inconel wall at the position marked "point A" on the sketch. The velocity and altitude histories of the test vehicle through the significant heating portion of flight (during which valid temperature data were recorded) are shown in Fig. 4. Using these trajectory data and the nose configuration of Fig. 3a, the laminar and turbulent heat rate, recovery enthalpy, and the local Reynolds number data of Fig. 5 were calculated by the methods of this paper (using the computer program NQLDW019.[1] The Prandtl-Meyer expansion method of obtaining local pressures was used.

These data were then input to a 10-element, one-dimensional structural heating program (NQLDW112)[11] to obtain the temperature histories shown as solid lines in Fig. 6. Note that the cases of a fully turbulent boundary layer and of transition at local Reynolds numbers of 2.8, 5.0, and 10.0 million are presented. The flight recorded temperature data are shown as circled points.

In general, the agreement between theory and flight data is quite good. The data indicate that transition from turbulent

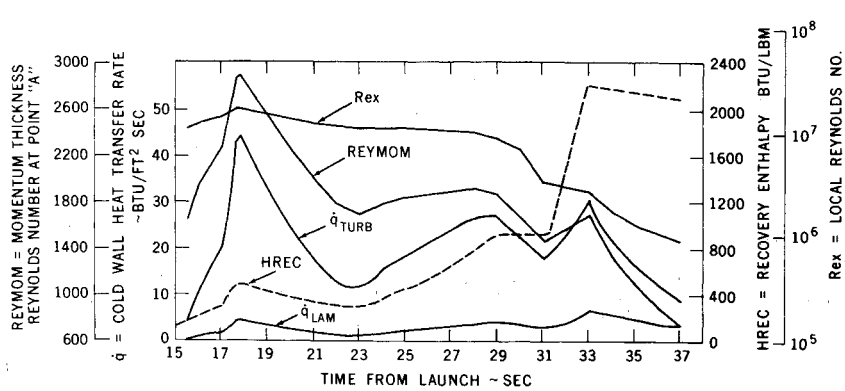

Fig. 5 Laminar and turbulent heat transfer rates, recovery enthalpy, local Reynolds number, and momentum thickness numbers at point A.

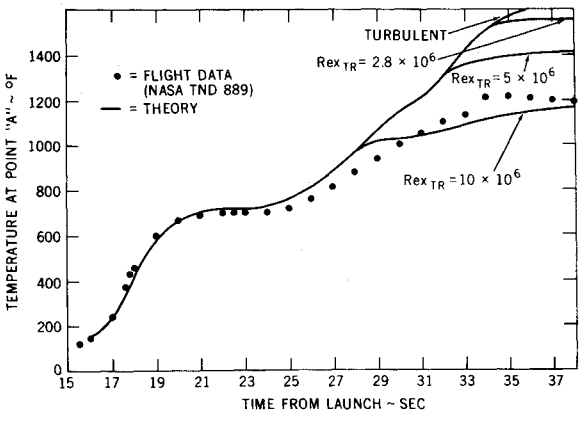

Fig. 6 Comparison of flight with theoretical data using the theory of NQL-DW019 to predict the heat rate history.

to laminar flow probably occurred at a calculated local Reynolds number of 7–8 million. It is emphasized that this local Reynolds number is defined as

$$Re_{x_{(Tr)}} = (\rho_{(x)} V_{(x)} X)/\mu_{(x)} \tag{30}$$

where the sub x values are taken at the outer edge of the boundary layer at point A. Inasmuch as the manner of approximating the effects of the entropy gradient through the shock layer results in more or less fictitious values of the local entropy at any given point, caution must be used in comparing the transition Reynolds number as defined by Eq. (30) with transition Reynolds numbers from other sources which do not make the same local entropy value assumptions.

2) Comparison with Flight Data from Black Brant VC Flight 21.006 GT

The vehicle nose of Fig. 3b was flown on Flight 21.006 GT, a Black Brant VC, and two thermocouples were located on the inner surface of the 0.062 in. stainless steel wall at the positions indicated as TC #1 and TC #9 in the sketch. The trajectory used in the calculations is taken from radar data and the velocity and altitude histories are shown in Fig. 7. The digital program (NQLDW019) was used to derive the heat transfer rate data of Figs. 8a and b for TC #1 and TC #9, respectively. These data, again using the structural heating analysis of Ref. 11, result in the temperature predictions (solid lines) of Figs. 9a and b.

If transition from turbulent to laminar flow is assumed to occur at a local Reynolds number of 10 million at TC #1,

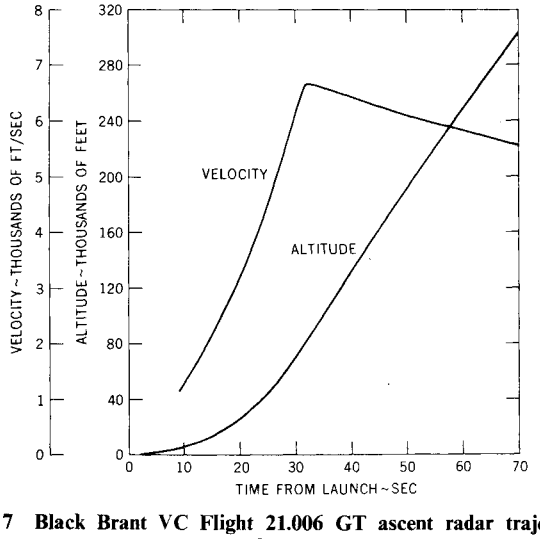

Fig. 7 Black Brant VC Flight 21.006 GT ascent radar trajectory data.

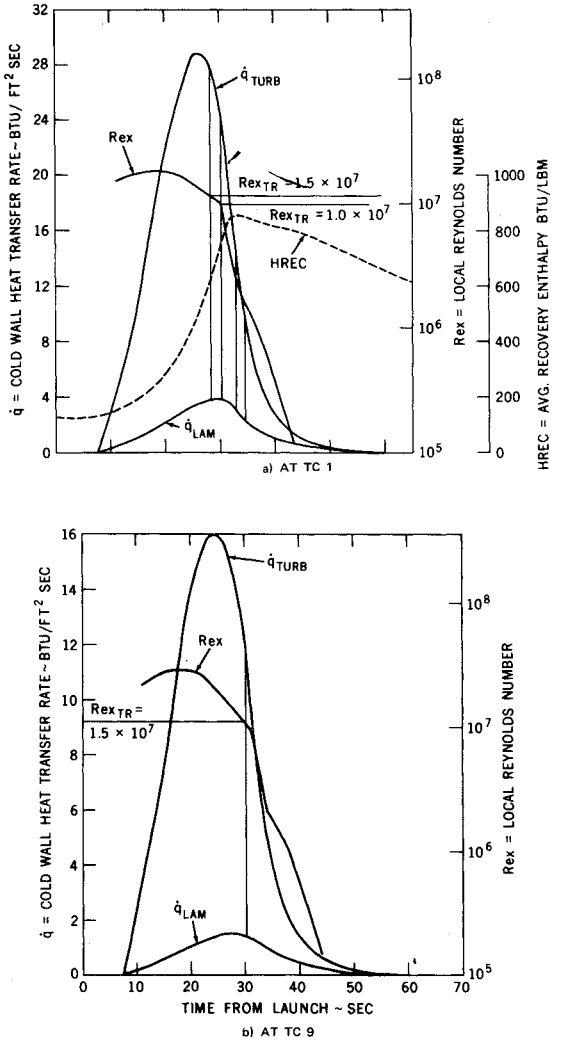

Fig. 8 Black Brant VC Flight 21.006 GT heat transfer rate data.

the agreement between theory and flight is seen to be extremely good (Fig. 9a). Similarly, the assumption of a transition Reynolds number of 15 million at TC #9 results in good agreement between theory and measurement.

Transition Reynolds Number

The ability to predict the heat-transfer rate is primarily dependent upon the ability to predict the nature of the local boundary layer. This holds true whether the analytic approach be approximate (as in the present case) or involves a complete numerical solution of the boundary-layer equations. Figures 6, 9a, and 9b indicate that the present analysis is adequate if the transition can be predicted. Accordingly, an empirical method for predicting the transition Reynolds number is sought by the simple expedient of recording experimental values as they are inferred by comparison of heating analysis predictions with the flight temperature data as has just been demonstrated.

Such a comparison is shown in Fig. 10. Of course, with the scant amount of data available the ability to predict transition Reynolds numbers for all tangent ogives at all flight conditions is almost totally absent. On the other hand, it should be borne in mind that the flight regimes, degrees of bluntness of the ogives, and general body surface conditions for large families of sounding rockets are sufficiently restricted as to make such an empirical approach quite practicable. In the present case (Fig. 10), only thin-wall metallic ogives are represented. It is quite likely that low conductivity noses (i.e., fiberglass phenolic) would have appreciably different ratios of external surface to local recovery

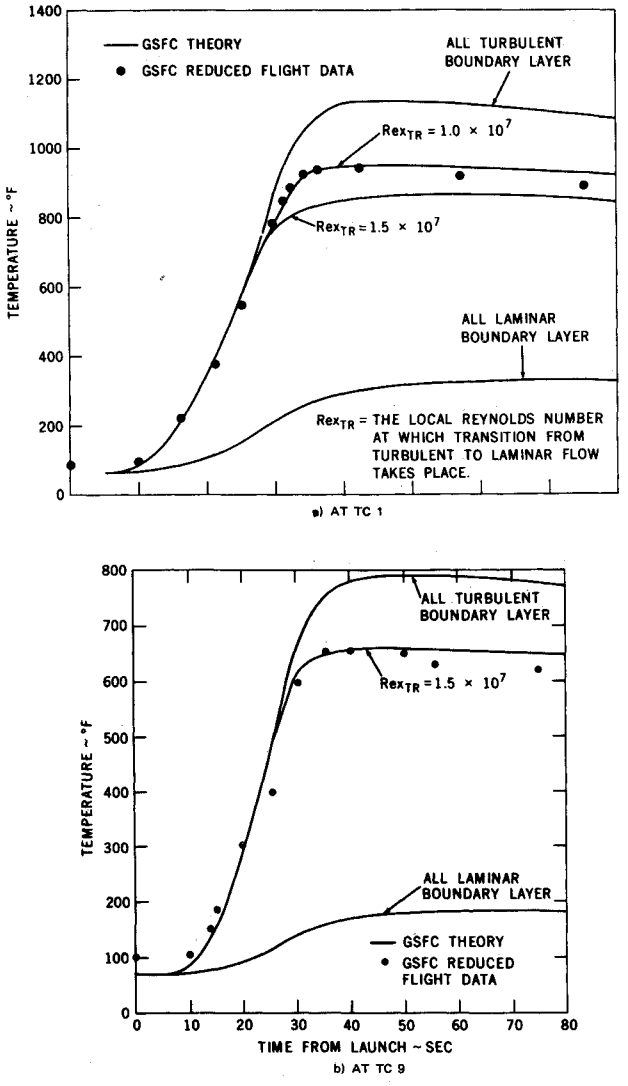

Fig. 9 Black Brant VC Flight 21.006 GT temperature of 0.062 in. stainless steel wall at TC9.

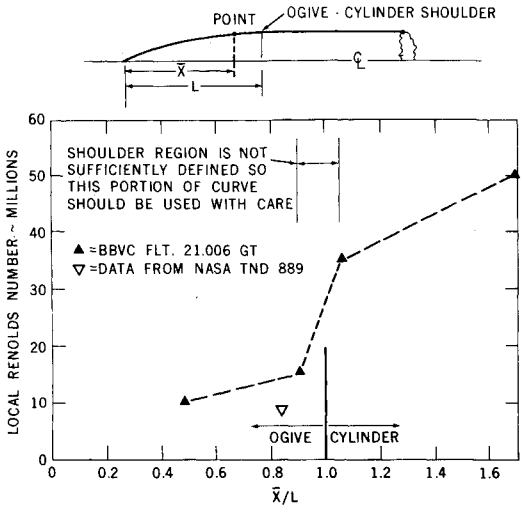

Fig. 10 Summary of transition local Reynolds number which best matches flight temperatures with present theoretical predictions.

temperatures and thence would be expected to require a separate curve such as that of Fig. 10. Over a period of time then, the use of the present theory should reasonably quickly allow an investigator to attain an adequate ability to predict the effects of aerodynamic heating on any tangent ogive nose.

Conclusions

The following conclusions are drawn from the work reported.

1) The tangent ogive aeroheating analysis methods described are capable of providing adequate predictions of the aerothermal effects on tangent ogive noses of typical sounding rockets through ascent.

2) The accuracy with which these predictions can be made is dependent primarily upon the accuracy with which transition from turbulent to laminar flow (in ascent) or laminar to turbulent flow (in re-entry) can be predicted. The extreme complexity of the boundary-layer transition phenomenon suggests that the empirical approach is the most practical at this time, particularly when large numbers of similar vehicles are involved, as is often the case with sounding rockets.

References

[1] Wing, L. D., "Tangent Ogive Nose Aerodynamic Heating Program: NQLDW019," Doc. X-742-71-161, April 1971, NASA.

[2] Wing, L. D., "Digital Utilization Program FM147—General Aerodynamic Heating," Rept. ER-109, Oct. 1967, Technical Services Div., Fairchild Hiller Corp., Germantown, Md.

[3] Wing, L. D., "Aerodynamic Heating for Wedge/Wedge or Cone/Cone at Angles-of-Attack from Zero to Approximately 40°," Rept. ER-116, Nov. 1968, Technical Services Div., Fairchild Hiller Corp., Germantown, Md.

[4] Hansen, C. F., "Approximations for the Thermodynamic and Transport Properties of High Temperature Air," TR R-50, 1959, NASA.

[5] Eckert, E. R. G. and Tewfik, O. E., "Use of Reference Enthalpy in Specifying the Laminar Heat Transfer Distribution around Blunt Bodies in Dissociated Air," *Journal of the Aero/Space Sciences*, Vol. 27, No. 6, June 1960, p. 464.

[6] Libby, P. A. and Cresci, R. J., "Evaluation of Several Hypersonic Turbulent Heat Transfer Analyses by Comparison with Experimental Data," TN 57-72, ASTIA Doc. AD 118093, July 1957, Wright Air Development Center, Wright Patterson Air Force Base, Ohio.

[7] Cohen, C. B. and Reshotko, E., "Similar Solutions for the Compressible Laminar Boundary Layer with Heat Transfer and Pressure Gradient," Rept. 1293, 1956, NACA.

[8] Fay, J. A. and Riddell, F. R., "Theory of Stagnation Point Heat Transfer in Dissociated Air," *Journal of the Aero/Space Sciences*, Vol. 25, No. 2, Feb. 1958, p. 73.

[9] Research Staff, "Equations, Tables, and Charts for Compressible Flow," Rept. 1135, 1953, NACA.

[10] Bland, W. M., Jr. and Collie, K. A., "Free Flight Aerodynamic Heating Data to Mach Number 10.4 for a Modified Von Karman Nose Shape," TND 889, May 1961, NASA.

[11] Wing, L. D., "10 Element One-Dimensional Structural Heating Programs," Doc. X-721-69-454, Aug. 1969, NASA.